JOURNAL OF MATERIALS SCIENCE **36** (2001) 5871 – 5879

Thermal and vapor pressure effects on cavitation and void growth

T. F. GUO, L. CHENG*
Department of Mechanical and Production Engineering, National University of Singapore, 10 Kent Ridge Crescent, Singapore 119260
E-mail: mpecl@nus.edu.sg

Vapor pressure and thermal stress induced growth and coalsecence of microvoids near interfaces of die/die-attach and die-pad/moulding compound is recognised as the precursor to interface delamination and popcorn cracking of plastic electronic packages. When exposed to humid ambient conditions prior to reflow soldering, plastic electronic packages absorb moisture, which condenses within the numerous micropores in the substrate, die attach, moulding compounds and in the vicinity of interfaces joining the different material layers. During reflow soldering, moisture in these micropores is vaporized. A representative material cell containing a single microvoid is used to investigate void growth under combined vapor pressure and thermal stress. A critical surface traction, the sum of the internal vapor pressure and the externally applied stress, defines the onset of unstable void growth. Existence of "large" microvoids lowers significantly the critical stress levels for unstable void growth. These stress levels are consistent with generally accepted estimates of stress levels for popcorn cracking given in the literature. Vapor pressure effects can be incorporated into a continuum description of stresses and strains and the Gurson-Tvergaard void growth model providing a new capability for full-field analysis of popcorn cracking in electronic packages.

1. Introduction

Moisture-induced popcorn failure is a common type of failure that occurs during surface mounting of electronic packages onto printed circuit board. During the reflow soldering process, the entire plastic package is exposed to temperatures as high as 220°C. Under such temperatures, moisture absorbed by package evaporates generating high internal vapor pressures within microvoids [1, 2]. Fan and Lim [3] have listed four stages which lead to final popcorn failure. In stage 1 (preconditioning), the package absorb moisture from the environment, which condenses in micropores in the substrate, solder mask, die attach and along the interfaces. In stage 2, the condensed moisture vaporizes under the high temperature associated with the reflow process, generating high internal vapor pressure which causes microvoids to nucleate, grow rapidly and coalesce. As a result small interfacial delamination zones are initiated. In stage 3, the vapor pressure exerts traction loading on the delaminated interfaces, aggravating the process of delamination and eventually causing the package to bulge. In the final stage, the interface crack (e.g. die/die-attach interface, die-pad/molding compound interface) propagates laterally outwards. When the crack reaches the package exterior, the high-pressure water vapor is suddenly released, producing an audible sound like popcorning. The popcorn cracking as a failure mechanism in electronics packages was first postulated by Fukuzawa *et al*. [1] in 1985 and has since stimulated numerous studies.

Previous works in this field focussing on moisture analysis have shed much light on moisture diffusion in electronics packages, e.g. the works of Tay and Lin [4] for thin quad flat packages (TQFP), and Galloway and Miles [5] for plastic ball grid array (PBGA) packages. In the latter a full-field FEA analysis was carried out to predict the moisture weight gain or loss in order to estimate the critical moisture concentration leading to die-die attach interface delamination. By contrast, similar in-depth mechanical analysis of popcorn failure is scarce. One such study was carried out by Fan and Lim [3], wherein, a representative volume element is introduced to estimate the vapor-pressure induced voiding effects on delamination. By far, studies to date assumed a pre-existing macroscopic crack prior to reflow soldering, and the vapor pressure is taken as traction loading on the delaminated crack [6–8].

The critical role of hydrostatic pressure on cavitation instability and cavity coalescence has been studied by Ball [9], Huang *et al*. [10], Hou and Abeyaratne [11], and Faleskog and Shih [12]. In a related study of interface delamination between the die-pad and the molding compound, Liu *et al*. [13] introduced a micromechanics model for the effective vapor pressure acting on the interfaces taking account of the evolving (interfacial) void volume fraction.

*Author to whom all correspondence should be addressed.

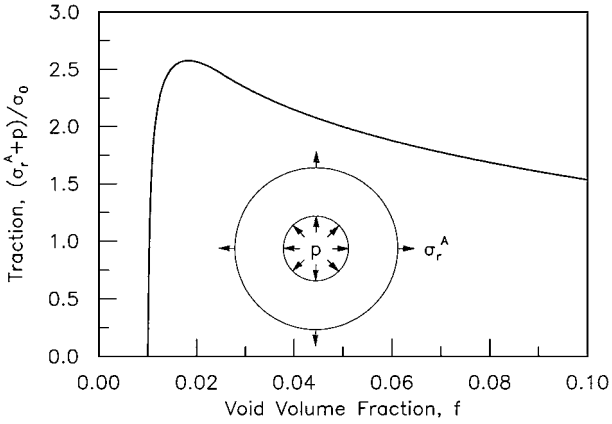

Figure 1 Traction applied to cavity in a finite matrix vs. evolution of void volume fraction $f(f_0 = 0.01, \varepsilon_0 = 0.01, N = 0)$. The microvoid is subjected to internal vapor pressure p and the externally applied radial stress σ_r^A.

The above studies taken together offers compelling evidence of vapor-pressure-induced void initiation, growth and coalescence as a key mechanism of catastrophic failure like popcorn cracking. In this study, we seek to understand the prototype of an instability event which is the precursor to the rapid interface delamination resulting in popcorn cracking. Thermal-stress induced voiding in electronic packages was considered by Huang *et al*. [14]. Indeed their result can be extended to include vapor pressure effects. This development is one of several findings reported in the present investigation.

Section 2 of this paper, treats a spherical cavity in a finitely deformed elasticplastic solid which is subjected to internal vapor pressure p and externally applied radial stress σ_r^A (see Fig. 1). Under the combined loading, $p + \sigma_r^A$, there is a critical surface traction which defines the maximal allowable pressure before the occurrence of unstable void growth and rupture. Moisture analysis by Fan and Lim [3] suggests common polymeric materials used in IC packages have void volume fractions ranging from 1% to 5%. The presence of such large initial voids, lowers significantly the critical surface traction to about 2–3 times the uniaxial yield stress of the polymer. These stress levels are within the previously estimated stress range for driving popcorn failure in plastic packages.

In Section 3, a model of vapor pressure which takes into account the mechanical-thermal coupling of the microvoid cell is proposed. Moisture concentrations and porosities enter into the modeling. Arising from finite thermal expansion, the vapor pressure-temperature relationship exhibit a non-monotonic behavior. In Section 4, the microvoid cell is homogenized to give a continuum description of important physical quantities. At the macroscopic level, the contribution of vapor pressure to the mean stress takes the factor form: $(1 - f)p$, where f is the current volume fraction of voids. Finally, in Section 5, the Gurson-Tvergaard model [15, 16] is extended to incorporate vapor pressure effects. The latter is suitable for implementation into a finite element code. This adds a new capability for full-field analysis of popcorn cracking problems.

2. Critical surface traction of a microvoid cell

The moisture absorbed by the plastic electronic packages is trapped in numerous tiny pores (or micro-voids). During surface mounting, the temperature of the package is raised to about 220°C, which is sufficient to evaporate the condensate with the micro-voids. Thus, the microvoids are subjected to internal vapor pressure p and remote stress σ_{ij}^A that characterizes the thermal stress imposed by the surrounding substrates. For the purpose of analysis, it is convenient to treat a spherical volume of material containing a microvoid of spherical shape with initial radius R_1. The matrix material is incompressible and the outer radius of the thick-walled sphere has initial radius R_2. The inner radial surface is subjected to internal vapor pressure p; a radial stress σ_r^A is applied to outer radius (see insert in Fig. 1).

Under the action of p and σ_r^A, the spherical volume deforms to the current inner radius r_1 and current outer radius r_2. The voided sphere is geometrically characterized by the initial and current void volume fractions f_0 and f:

$$f_0 = \left(\frac{R_1}{R_2}\right)^3, \qquad f = \left(\frac{r_1}{r_2}\right)^3. \tag{2.1}$$

Theoretical estimates by Fan and Lim [3] show that the initial void volume fraction ranges from 1% to 5% for some polymeric materials commonly used in IC packages; for example, $f_0 = 1.4\%$ for mold compound and $f_0 = 3.46\%$ for die attach.

The matrix material of the microvoid cell is assumed to be an isotropic, incompressible elastic plastic solid with uniaxial relation between true stress and logarithmic strain given by $\sigma/\sigma_0 = H(\varepsilon)$, where σ_0 is the yield stress. The radial equilibrium solution for a spherically symmetric cell is then found to be (see the Appendix A, Equation A.13)

$$\frac{\sigma_r^A + p}{\sigma_0} = \int_{\varepsilon_1}^{\varepsilon_2} \frac{H(\varepsilon)\,\mathrm{d}\varepsilon}{1 - \exp\left(-\frac{3}{2}\varepsilon\right)} \tag{2.2}$$

where ε_1 and ε_2 are the radial strains at the two-end points of the cell, which can be determined solely by the current and initial void volume fractions:

$$\varepsilon_1 = \frac{2}{3}\ln\left(\frac{f_0}{f}\frac{1-f}{1-f_0}\right), \quad \varepsilon_2 = \frac{2}{3}\ln\left(\frac{1-f}{1-f_0}\right). \tag{2.3}$$

Fig. 2 displays the curves of void volume increase with applied traction $\sigma_r^A + p$ for several (nonzero) initial void fractions. It can be seen that the applied traction increases continuously from zero to its peak value and then decreases. For a defect-free solid, $f_0 = 0$, the integral in (2.2) defines the so-called cavitation stress [9–12]. It is the threshold stress for a void to nucleate and then grow rapidly. The cavitation stress is indicated by the intersection of dotted line, in Fig. 2, with the vertical axis. The dotted line represents the asymptote for the trajectories of void volume vs. stress for nonzero initial void fractions.

A point to note is that for an initially "defect-free" solid, the critical cavitation stress level is very high, e.g.,

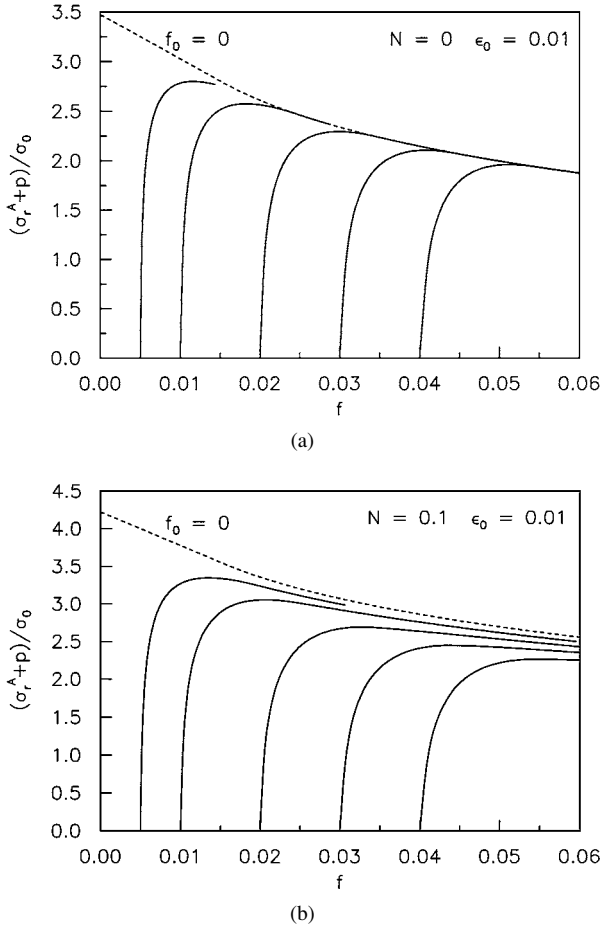

Figure 2 Traction $\sigma_r^A + p$ vs. current void volume fraction f for f_0 equal 0.005, 0.01, 0.02, 0.03, 0.04 with $\varepsilon_0 = 0.01$. (a) $N = 0$; (b) $N = 0.1$. The dotted lines give the result for $f_0 \to 0$.

about $3.5\sigma_0$ for $N = 0$, and about $4.2\sigma_0$ for $N = 0.1$. However, this critical stress level is significantly lowered by the larger voids already existing in the plastic IC packages, whose fractions range from 1% to 5% as noted earlier.

In summary, the critical surface traction σ_c, given by the peak value of each curve, defines the maximal allowable pressure before the cell "bursts". For highly constrained ductile components (e.g. the die-attach) in electronic packages, a local stress-based design criterion may take the form

$$\sigma_r^A + p \le \sigma_c. \tag{2.4}$$

This criterion applies to failure by voiding, such as the rapid nucleation and growth of voids.

3. Vapor pressure modeling

The foregoing analytic results provide an understanding of the evolution of microvoid under prescribed tractions σ_r^A and p. In this section, thermal effects are incorporated in the modeling of vapor pressure.

3.1. Thermal expansion

Thermal strain has no effect on the stress-strain relation in Equation A.6. Hence Equation 2.2 along with the integration limits (2.3) remains valid if thermal expansion is considered. Thermal expansion, however, affects geometrical relations.

Let α be the thermal expansion coefficient and ΔT the temperature rise. The incompressibility reads

$$\varepsilon_r + \varepsilon_\theta + \varepsilon_\phi - 3\alpha\Delta T = 0. \tag{3.1}$$

Substitution of the logarithmic strains (A.3) leads to

$$\frac{dr}{dR} = \left(\frac{R}{r}\right)^2 e^{3\alpha\Delta T}$$

whose solution is given by

$$r^3 = \left(R^3 - R_1^3\right) e^{3\alpha\Delta T} + r_1^3. \tag{3.2}$$

With the definition of f in Equation 2.1, we have

$$f = \frac{\rho^3}{\frac{1-f_0}{f_0} e^{3\alpha\Delta T} + \rho^3} \quad \text{or} \quad \rho = e^{\alpha\Delta T} \sqrt[3]{\frac{f}{f_0}\frac{1-f_0}{1-f}} \tag{3.3}$$

where $\rho = r_1/R_1$ is the growth ratio of the void radii. We may take f_0, f and ΔT as basic quantities of the void. Thus, the lower and upper limits of the integration (2.2), ε_1 and ε_2 in (2.3), are independent of temperature. For future use we compute the ratio of the current volume V to the initial volume V_0, of the void cell. This relation can be obtained from a simple manipulation

$$\frac{V}{V_0} = \frac{r_2^3}{R_2^3} = (1 - f_0)e^{3\alpha\Delta T} + f_0\rho^3 = \frac{1 - f_0}{1 - f} e^{3\alpha\Delta T}. \tag{3.4}$$

3.2. Vapor pressure for fully vaporized moisture

Consider a small representative material sample (microvoid cell) of volume dV which contains a microvoid of void volume dV_f. The vapor pressure p at a fully vaporized state obeys the ideal gas law [3, 17], given as follows

$$p dV_f = dmRT \tag{3.5}$$

where R is the universal gas constant (=8.314 J/mol), dm the moisture weight within the microvoid, and T the temperature in K. Dividing both sides of Equation 3.5 by dV leads to

$$pf = CRT \tag{3.6}$$

where $C = dm/dV$ is the local moisture concentration after preconditioning and $f = dV_f/dV$ is the void volume fraction. Equation 3.6, supplemented by moisture diffusion analysis [4, 5], permits us to evaluate the initial volume fraction f_0 of the void.

The two states (p, f, T, C) and (p_0, f_0, T_0, C_0) are related by

$$\frac{p}{p_0} = \frac{T f_0 C}{T_0 f C_0}. \tag{3.7}$$

During deformation ($dV_0 \to dV$) associated with a temperature rise ΔT ($= T - T_0$), the moisture weight dm is assumed conserved. Hence

$$\frac{p}{p_0} = \frac{T}{T_0}\frac{f_0}{f}\frac{dV_0}{dV}. \tag{3.8}$$

From (3.4), the relative volume change dV/dV_0 of the microvoid cell during mechanical deformation and thermal expansion is

$$\frac{dV}{dV_0} = \frac{1-f_0}{1-f}e^{3\alpha\Delta T}. \tag{3.9}$$

Combining Equations 3.8 and 3.9 gives

$$\frac{p}{p_0} = \frac{T}{T_0}\frac{f_0}{f}\frac{1-f}{1-f_0}e^{-3\alpha\Delta T}. \tag{3.10}$$

It is noted that the vapor pressure depends on temperature and void volume fraction. With given values of f and f_0, the vapor pressure p attains the maximum value $p_{\max}$ at the critical temperature $T_c = 1/3\alpha$:

$$p_{\max} = p_0\frac{\exp(3\alpha T_0 - 1)}{3\alpha T_0}\frac{f_0}{f}\frac{1-f}{1-f_0}, \tag{3.11}$$

Using this, Equation 3.10 can be rewritten as

$$\frac{p}{p_{\max}} = 3\alpha T\exp(1 - 3\alpha T). \tag{3.12}$$

Fig. 3 shows the relationship between the normalized vapor pressure $p/p_{\max}$ and the normalized temperature $3\alpha T$. The occurrence of the peak pressure $p_{\max}$ is due to finite thermal expansion of the cell (see Equation 3.9). This peak value, however, cannot be reached in general. Consider for example, the die attach, with $\alpha = 1.5 \times 10^{-4}$. The use of (3.12) gives a critical temperature of $T_c = 1949$°C, which is much higher than the surface mounting temperature of about 220°C. The vapor pressure p can thus be considered to be a monotonically increasing function of temperature during surface mounting. For the die attach, the vapor pressure ratio $p/p_{\max}$ is about 0.48. Increasing the temperature from the room temperature of 25°C to 220°C causes an increase in the vapor pressure in the die attach by 3.14 times when void volume fractions remain unchanged, as can be deduced in Equation 3.10.

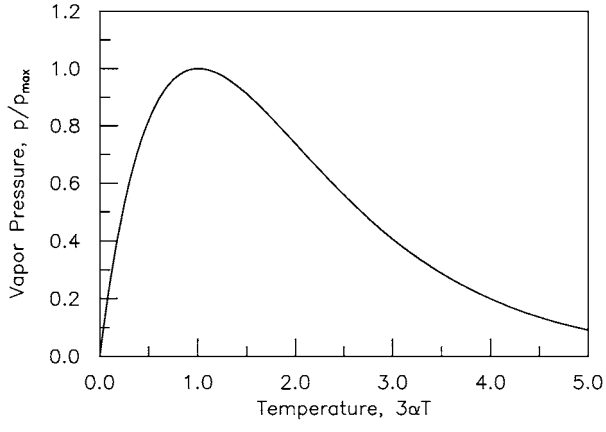

Figure 3 Behavior of moisture-induced vapor pressure in a microvoid cell vs. temperature.

3.3. Two-phase vapor pressure

In the previous section, a relationship between the internal vapor pressure p, the void volume fraction f and temperature T has been obtained under the assumption that the moisture in a microvoid is fully vaporized at T between the preconditioning temperature T_0 and the peak reflow temperature T_r ($T_0 \le T \le T_r$). For non-fully vaporized moisture, however, water and vapor gas phases coexist. To describe this two-phase moisture, one should determine the transition temperature T_c at which the moisture in voids is fully saturated in vapor phase, and then identify three distinct cases at which vapor pressure may be computed [3]. The first case is when the moisture density in the voids is low enough such that all the moisture becomes vaporized at preconditioning temperature T_0; i.e. $T_c \le T_0$. This was the case treated above.

In the second case, the moisture is fully vaporized at a temperature between preconditioning T_0 and the peak reflow temperature T_r; i.e. $T_0 \le T_c \le T_r$. In the last case, the moisture is not fully vaporized even at reflow temperature T_r; i.e. $T_c \ge T_r$. For these two cases, strong nonlinearities are found among vapor pressure, thermal expansion and the transition temperature, which will make the formulation cumbersome. We leave this topic for future study.

4. Homogenization: a continuum description

Let V_M and V be the matrix and cell volumes, respectively. For the spherical shell under study, $V_M = 4\pi(r_2^3 - r_1^3)/3$ and the micro volume element is $dv = 4\pi r^2 dr$. We thus have

$$\frac{dv}{V} = f\frac{dr^3}{r_1^3} = \frac{3}{2}\frac{f-f_0}{1-f_0}\frac{e^{\frac{3}{2}\varepsilon}\,d\varepsilon}{\left(1-e^{\frac{3}{2}\varepsilon}\right)^2} \tag{4.1}$$

where ε signifies the radial strain ε_r given in (A.9). Recall that volume averaging of microscopic fields gives the macroscopic counterparts; e.g. for stress σ_i, the macroscopic stress Σ_i is defined by

$$\Sigma_i = \frac{1}{V}\int_{V_M}\sigma_i\,dv \qquad i = r, \theta, \phi \tag{4.2}$$

in the current configuration.

By (A.12), the macroscopic radial stress Σ_r is

$$\frac{\Sigma_r}{\sigma_0} = \frac{3}{2}\frac{f-f_0}{1-f_0}\int_{\varepsilon_1}^{\varepsilon_2}\frac{e^{\frac{3}{2}\varepsilon}\,d\varepsilon}{\left(1-e^{\frac{3}{2}\varepsilon}\right)^2}\int_{\varepsilon_1}^{\varepsilon}\frac{H(\tau)\,d\tau}{1-e^{-\frac{3}{2}\tau}} - \frac{(1-f)p}{\sigma_0}. \tag{4.3}$$

As the microscopic mean stress is defined as $\sigma_m = (\sigma_r + 2\sigma_\theta)/3$, the macroscopic mean stress is as follows:

$$\frac{\Sigma_m}{\sigma_0} = \frac{\Sigma_r}{\sigma_0} - \frac{f-f_0}{1-f_0}\int_{\varepsilon_1}^{\varepsilon_2} \frac{H(\varepsilon)\, e^{\frac{3}{2}\varepsilon}\, d\varepsilon}{\left(1-e^{\frac{3}{2}\varepsilon}\right)^2}$$

$$= \frac{f-f_0}{1-f_0}\left\{\frac{3}{2}\int_{\varepsilon_1}^{\varepsilon_2} \frac{e^{\frac{3}{2}\varepsilon}\, d\varepsilon}{\left(1-e^{\frac{3}{2}\varepsilon}\right)^2}\int_{\varepsilon_1}^{\varepsilon} \frac{H(\tau)\, d\tau}{1-e^{-\frac{3}{2}\tau}} - \int_{\varepsilon_1}^{\varepsilon_2} \frac{H(\varepsilon)\, e^{\frac{3}{2}\varepsilon}\, d\varepsilon}{\left(1-e^{\frac{3}{2}\varepsilon}\right)^2}\right\} - \frac{(1-f)p}{\sigma_0}. \quad (4.4)$$

In order to arrive at the above expression, the equation $(\sigma_r - \sigma_\theta)/\sigma_0 = H(\varepsilon_r)$ is used. It is interesting to note that the vapor pressure p appears in the above expression for the macroscopic mean stress Σ_m, with a scaling factor of $(1-f)$. This proves to be useful in extending the Gurson model [15] to incorporate the effect of vapor pressure. The microscopic Mises stress is defined as $\sigma_e = |\sigma_r - \sigma_\theta|$; the corresponding macroscopic quantity is as follows:

$$\frac{\Sigma_r - \Sigma_\theta}{\sigma_0} = \frac{3}{2}\frac{f-f_0}{1-f_0}\int_{\varepsilon_1}^{\varepsilon_2} H(\varepsilon)\frac{e^{\frac{3}{2}\varepsilon}\, d\varepsilon}{\left(1-e^{\frac{3}{2}\varepsilon}\right)^2}. \quad (4.5)$$

Invoking incompressibility, the microscopic effective strain is $\varepsilon_e = \frac{2}{3}|\varepsilon_r - \varepsilon_\theta| = |\varepsilon_r|$ and $\varepsilon_r = -2\varepsilon_\theta$. Averaging ε_r leads to

$$E_r = -2E_\theta = \frac{1}{V}\int_{V_M} \varepsilon_r\, dv = \frac{3}{2}\frac{f-f_0}{1-f_0}\int_{\varepsilon_1}^{\varepsilon_2} \frac{\varepsilon e^{\frac{3}{2}\varepsilon}\, d\varepsilon}{\left(1-e^{\frac{3}{2}\varepsilon}\right)^2}$$

$$= \frac{2}{3(1-f_0)}\left\{\ln\frac{1-f}{1-f_0} + f_0 \ln\frac{1-f_0}{f_0(1-f)} + f\ln\frac{f(1-f_0)}{1-f} + ff_0\ln\frac{f_0(1-f)}{f(1-f_0)}\right\} \quad (4.6)$$

It is readily deduced that $\lim_{f\to 1} E_r = 0$, inferring that the macroscopic effective strain, $|E_r|$, at final rupture is zero. It also implies that E_r is not a monotonically increasing function of f. As the void grows (f increases), there exists an extremum for E_r (or E_θ) if f satisfies the following condition

$$f_c = \frac{1}{1 + f_0^{\frac{f_0}{1-f_0}} - f_0^{\frac{1}{1-f_0}}}. \quad (4.7)$$

Equation 4.7 describes a family of critical void fractions with the minimum f_c^* corresponding to f_0 approaching zero:

$$f_c^* = \lim_{f_0\to 0} f_c = \frac{1}{2}. \quad (4.8)$$

Correspondingly, E_θ attains the maximum E_θ^*:

$$E_\theta^* = \lim_{f_0\to 0} E_\theta\big|_{f=\frac{1}{2}} = \frac{1}{3}\ln 2 \quad (4.9)$$

where

$$\lim_{f_0\to 0} E_\theta = -\frac{1}{3}[f\ln f + (1-f)\ln(1-f)]. \quad (4.10)$$

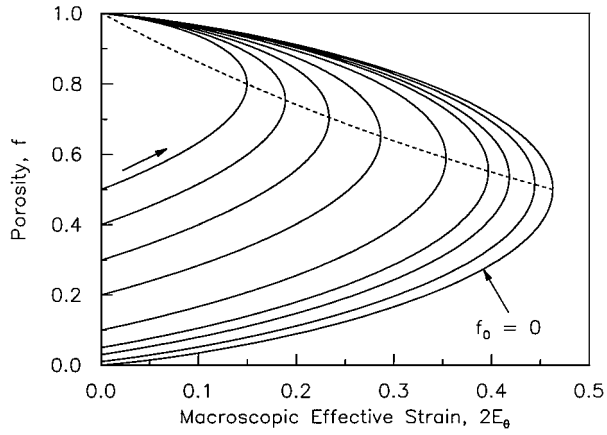

Figure 4 Evolution of f relative to the effective macroscopic strain, $2E_\theta$, for several different f_0. For each f_0, E_θ has a maximum. The dotted line is the trajectory joining the maximum of various f_0.

Thus, one may conclude that during the course of void growth, E_θ is finite with a limit ($\frac{1}{3}\ln 2$), irrespective of the evolution law of f.

Fig. 4 shows the trajectory of f versus the macroscopic effective strain $2E_\theta$, where the curve corresponding to $f_0 = 0$ is governed by Equation 4.10, and the dotted line is the trajectory joining the maxima of E_θ for various initial void volume fractions. Since $\lim_{f\to 1} E_\theta = 0$, any trajectory in the (f, E_θ)-space will be terminated at the point (1, 0).

It is worthwhile to make a few remarks on (4.7). In the current use of the Gurson model [15], one needs to know the critical porosity for the onset of coalescence and for final material failure. Here, depending on the initial state, the critical porosity f_c given in (4.7) has a minimum value $f_c^* = \frac{1}{2}$ when the initial porosity approaches zero, and to the value $f_c^* = \frac{1}{2}$ there corresponds the maximum effective strain $2E_\theta^*$. Hence for the single void under study (without void interactions), we may take f_c^* as the void volume fraction at final fracture: $f_F = f_c^* = \frac{1}{2}$. With void interactions, the value f_F will be much lower than f_c^*. Studies by Tvergaard and Needlemann [18] have indicated that f_F is about 0.25.

In the above homogenization, we obtain three macroscopic invariants, the mean stress Σ_m, the Mises stress $\Sigma_\theta - \Sigma_r$, and the effective strain $2E_\theta$. In the state space spanned by them, one can envision the evolution of void volume fractions. Figs 5 and 6 show three sections in state spaces; Fig. 5 focuses on the influence of the initial void volume fraction f_0 while Fig. 6 focuses on the effect of hardening of N. In these figures, ε_0 is set to be 1 percent and f is taken to be a flow parameter beginning with a certain initial value f_0 and ending with $f = 1$. The hardening exponent is taken as $N = 0.1$ in Fig. 5 while the initial fraction is taken as $f_0 = 0.01$ in Fig. 6.

Fig. 5a shows the behavior in the stress space. High stress triaxiality is observed in the early stage of the void growth. From Fig. 5b and c, one can easily see that the initial value f_0 of f has significant effect on the flow before effective strain $2E_\theta$ attains its maximum value. After the maximum strain is reached, the effect of f_0 diminishes and becomes negligible as f approaches $f = 1$. In the very early stage of the flow, the mean stress

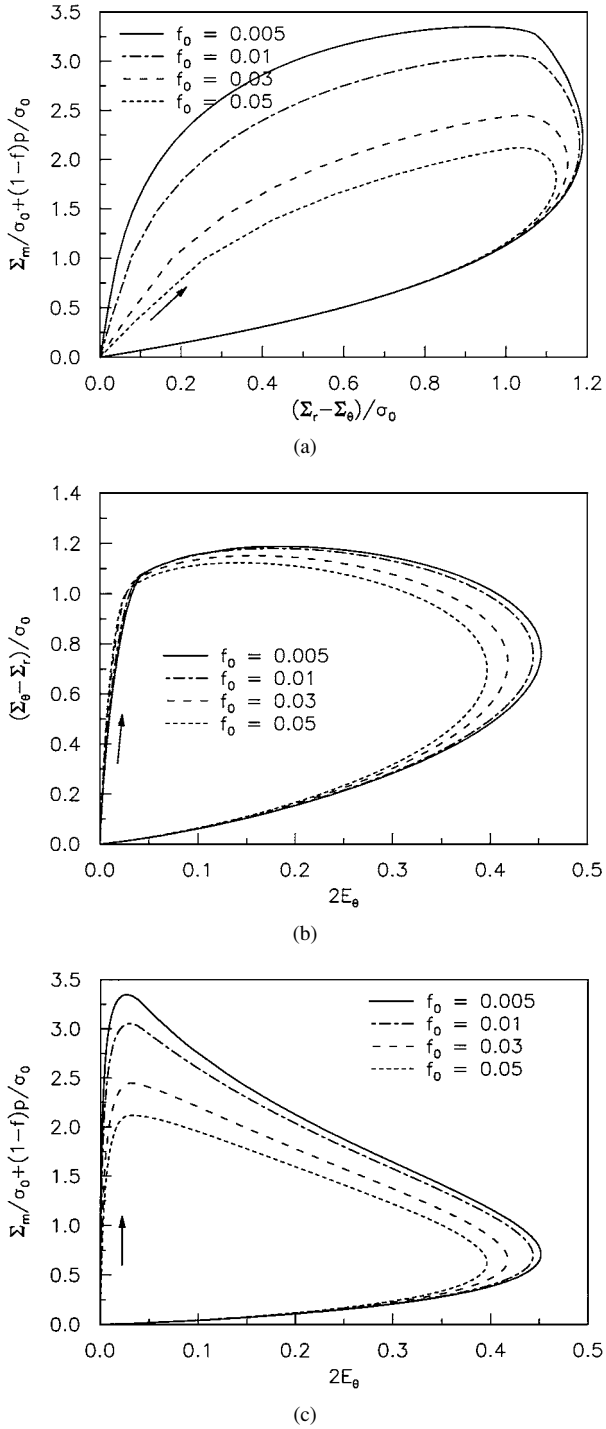

Figure 5 Evolution in the macroscopic state space spanned by effective stress, $\Sigma_\theta - \Sigma_r$, mean stress plus vapor pressure, $\Sigma_m + (1-f)p$, and effective strain, $2E_\theta$ for $f_0 = 0.005$, 0.01, 0.03, 0.05; $N = 0.1$ and $\varepsilon_0 = 0.01$. (a) Section of $\Sigma_\theta - \Sigma_r \sim \Sigma_m + (1-f)p$, (b) section of $\Sigma_\theta - \Sigma_r \sim 2E_\theta$ and (c) section of $\Sigma_m + (1-f)p \sim 2E_\theta$.

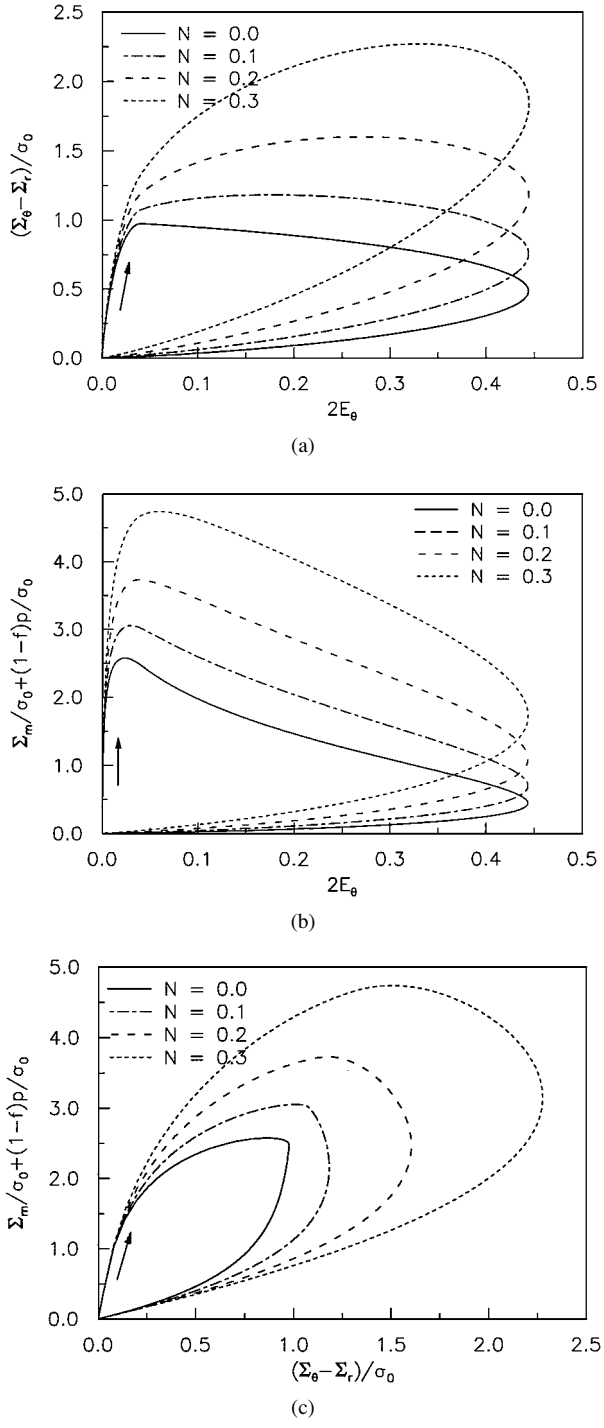

Figure 6 Evolution in the macroscopic state space spanned by effective stress, $\Sigma_\theta - \Sigma_r$, mean stress plus vapor pressure, $\Sigma_m + (1-f)p$, and effective strain, $2E_\theta$, for $N = 0.0$, 0.1, 0.2 and 0.3, $\varepsilon_0 = 0.01$. (a) Section of $\Sigma_\theta - \Sigma_r \sim 2E_\theta$ and (b) section of $\Sigma_m + (1-f)p \sim 2E_\theta$, and (c) section of $\Sigma_\theta - \Sigma_r \sim \Sigma_m + (1-f)p$.

together with vapor pressure attains its maximum; it decreases rapidly thereafter towards its zero state after crossing the turning point where $2E_\theta$ is maximal (see Fig. 5c). The effective stress, however, has a relatively smooth change with increasing $2E_\theta$, so the maximal point is not as pronounced as in the case of the mean stress (see Fig. 5b).

Since the effective strain $2E_\theta$ depends only on void fractions, the hardening parameter N affects only the stress level, but not the deformation. For a given initial void volume fraction, the deformation is limited by the maximal effective strain. With an increase in the effective strain from zero to its maximum value of about 0.43, the effective stress increases almost monotonically, with different hardening exponent effecting different patterns of increase (Fig. 6a); in contrast, the mean stress displays a parallel decrease for different hardening exponent after attaining its maximum (Fig. 6b). The triaxiality for different exponent is approximately a constant, see Fig. 6c.

Fig. 7 displays the behavior of the macroscopic mean stress versus the current void volume fraction for

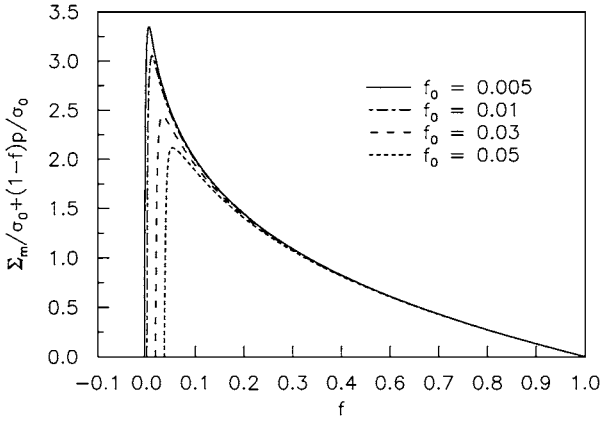

Figure 7 Behavior of macroscopic mean stress versus current void volume fraction for $f_0 = 0.005, 0.01, 0.03, 0.05$.

several values of f_0. The materials constants are those used to generate the results in Fig. 5.

5. Extension of the Gurson model

The preceding micromechanics analysis applies for proportional loadings of a spherically-symmetric cell. For multiaxial loadings, we provide a tentative modified Gurson model incorporating internal vapor pressure. The Gurson-Tvergarrd yield condition [15, 16] is given by

$$\Phi = \left(\frac{\Sigma_e}{\sigma_e}\right)^2 + 2q_1 f \cosh\left(\frac{3q_2\Sigma_m}{2\sigma_e}\right) - \left(1+q_3 f^2\right) = 0 \tag{5.1}$$

where Σ_e denotes the Mises equivalent macroscopic stress, Σ_m the mean macroscopic stress, σ_e the Mises equivalent stress of the matrix and f the current void fraction. Factors q_1, q_2 and q_3 were introduced by Tvergaard to improve the model predictions for periodic arrays of cylindrical and spherical voids.

A point to note is that the Gurson yield condition was derived originally from a cell containing a traction-free void, and the matrix is assumed to be rigid-plastic. Denoting the microscopic stress field of a traction-free void cell by σ^0_{ij}, the microscopic stress field σ_{ij} for a non-traction-free void cell is the superposition of internal pressure p and σ^0_{ij}:

$$\sigma_{ij} = -p\delta_{ij} + \sigma^0_{ij} \tag{5.2}$$

The above is exact, up to first order, as long as the void remains spherical throughout the deformation.

Recalling that macroscopic stress Σ_{ij} is defined as the average of the microscopic stress σ_{ij} over the cell, the following equation is obtained

$$\Sigma_{ij} = \frac{1}{V}\int_{V_M} \sigma_{ij}\,dv = (1-f)\frac{1}{V_M}\int_{V_M} \sigma_{ij}\,dv \tag{5.3}$$

where V is the cell volume, V_M is the matrix volume and f is the void volume fraction. Substitution of Equation 5.2 yields

$$\Sigma_{ij} = -(1-f)p\delta_{ij} + \Sigma^0_{ij} \tag{5.4}$$

and the mean macroscopic stress Σ_m is

$$\Sigma_m = \Sigma^0_m - (1-f)p. \tag{5.5}$$

Observe that Σ^0_{ij} and Σ^0_m are the macroscopic stresses corresponding to σ^0_{ij}. Therefore for a traction-free void cell the mean macroscopic stress Σ^0_m can be expressed in terms of Σ_m, p and f:

$$\Sigma^0_m = \Sigma_m + (1-f)p. \tag{5.6}$$

Since internal pressure has no effect on the Mises (macroscopic) stress, replacement of Σ_m by $\Sigma_m + (1-f)p$ in the Gurson-Tvergaard yield condition (5.1) gives the modified G-T model which is shown as follows

$$\Phi = \left(\frac{\Sigma_e}{\sigma_e}\right)^2 + 2q_1 f \cosh\left(\frac{3q_2[\Sigma_m + (1-f)p]}{2\sigma_e}\right) - \left(1+q_3 f^2\right) = 0. \tag{5.7}$$

It is noted that the contribution of vapor pressure to the (macroscopic) mean stress takes the factor form $(1-f)p$. A similar factor has appeared in the works of Fan [19] on the yield criterion for PMMA at a bone-implant interface. Herein the internal pressure p within the void is a function of void volume fraction f and temperature T, as given by (3.10).

The standard Gurson-Tvergaard relation has two internal variables, σ_e and f. The extended form introduces an additional variable p. The evolution rule for p obeys (3.12) for $T_c \le T_0$. More work is required to formulate the evolution rules for p encompassing the temperature range $T_0 \le T_c \le T_r$, and $T_c \ge T_r$. Nevertheless, the above (extended) Gurson model when implemented for finite element crack growth analysis in the manner of Xia and Shih [20, 21] could add new insights on phenomenon of popcorn cracking in electronic packages.

6. Concluding remarks

Theoretical results for a microvoid growth under both internal vapor pressure and external loading is obtained within the context of finite deformation. Under the combined loading, $p + \sigma^A_r$, there is a critical surface traction which defines occurrence of unstable void growth and rupture. The existence of large initial voids, void volume fractions ranging from 1% to 5%, lowers significantly the critical surface traction to about 2–3 times the uniaxial yield stress of the polymeric material. These stress levels fall within generally accepted estimates of the stress range associated with popcorn failure in plastic packages.

At a macroscopic level, the contribution of vapor pressure to the mean stress takes the factor form, $(1-f)p$, i.e. a fraction of vapor pressure. Homogenization of the cell also shows that the macroscopic effective strain is finite during the course of void growth and depends only on current void volume fraction.

A model of vapor pressure which takes into account the mechanical-thermal coupling of the microvoid cell is established. Moisture concentrations and porosities

enter into the modeling. Nonlinear behaviors of vapor pressure with temperature rise are revealed.

The Gurson-Tvergaard model has been extended to incorporate vapor pressure effects. The extended model is being implemented in a finite element code which will provide a new capability to perform full-field analysis of popcorn cracking in electronic packages.

Acknowledgments

The authors would like to thank Dr. X. J. Fan of Institute of Microelectronics, Singapore for many valuable discussions. The support of this work by the National University of Singapore (grant no. NUS-RP 3972710) is gratefully acknowledged.

A. Appendix

Let (R, Θ, Φ) denote the spherical coordinates of a point in the reference undeformed microvoid, and (r, θ, ϕ) denote the corresponding coordinates in the deformed cell. With spherically symmetric deformation,

$$r = \hat{r}(R), \quad \theta = \Theta, \quad \phi = \Phi.$$

The deformation gradient tensor $\mathbf{F}$ is

$$\mathbf{F} = \frac{\mathrm{d}\hat{r}}{\mathrm{d}R}\mathbf{e}_r \otimes \mathbf{e}_r + \frac{\hat{r}}{R}(\mathbf{e}_\theta \otimes \mathbf{e}_\theta + \mathbf{e}_\phi \otimes \mathbf{e}_\phi)$$

where $\mathbf{e}_r$,$\mathbf{e}_\theta$ and $\mathbf{e}_\phi$ forms an orthonormal basis for the spherical coordinate system (the two coordinate systems are assumed to coincide; e.g., $\mathbf{e}_R = \mathbf{e}_r$.) Incompressibility of the matrix gives

$$r^3 - r_1^3 = R^3 - R_1^3, \tag{A.1}$$

which is equivalent to the condition $\det([F_{ij}]) = 1$, or

$$\frac{\mathrm{d}\hat{r}}{\mathrm{d}R} = \left(\frac{R}{\hat{r}}\right)^2.$$

From (A.1), the current void volume fraction f can be written as

$$f = \frac{f_0\rho^3}{1 - f_0 + f_0\rho^3}$$

where $\rho = r_1/R_1$ signifies the growth ratio of the microvoid. The growth ratio ρ may be expressed in terms of the initial and current void volume fractions as

$$\rho = \sqrt[3]{\frac{f}{f_0}\frac{1 - f_0}{1 - f}}. \tag{A.2}$$

Therefore, any nondimensional quantities generated by r_1, r_2, R_1 and R_2 can be expressed in terms of f_0 and f.

As cavitation is a phenomenon of instability in materials, it is necessary to consider finite deformation of the solid. Invoking incompressibility condition equation (A.1), the true (logarithmic) strains, defined by the principal stretches in the respective directions, are

$$\varepsilon_\mathrm{r} = \ln\frac{\mathrm{d}r}{\mathrm{d}R}, \quad \varepsilon_\theta = \varepsilon_\phi = \ln\frac{r}{R}. \tag{A.3}$$

In the deformed configuration, the true (Cauchy) stress components in spherical coordinate system (r, θ, ϕ) are σ_r, σ_θ and σ_ϕ, which satisfy the following equilibrium equation

$$\frac{\mathrm{d}\sigma_\mathrm{r}}{\mathrm{d}r} + \frac{2}{r}(\sigma_\mathrm{r} - \sigma_\theta) = 0 \tag{A.4}$$

together with $\sigma_\phi = \sigma_\theta$. The boundary conditions are

$$\sigma_\mathrm{r}(r = r_1) = -p, \quad \sigma_\mathrm{r}(r = r_2) = \sigma_\mathrm{r}^\mathrm{A}. \tag{A.5}$$

It is noted that both p and $\sigma_\mathrm{r}^\mathrm{A}$ are Cauchy-type tractions applied at the void surface r_1 and at the outer boundary r_2 of the matrix, respectively.

Following the approach of Huang *et al*. [14], the matrix is assumed as an isotropic, incompressible elastic-plastic solid with a uniaxial relation between true stress and logarithmic strain given by

$$\frac{\sigma}{\sigma_0} = H(\varepsilon) \tag{A.6}$$

where σ_0 is the tensile yield stress. For an elastic-plastic power hardening solid, $H(\varepsilon)$ has the form

$$H(\varepsilon) = \begin{cases} \varepsilon/\varepsilon_0 & \text{if } |\varepsilon| < \varepsilon_0 \\ (|\varepsilon|/\varepsilon_0)^N \ \mathrm{sign}\ (\varepsilon) & \text{if } |\varepsilon| \geq \varepsilon_0 \end{cases} \tag{A.7}$$

where $\varepsilon_0 = \sigma_0/E$ is the reference strain, E the Young's modulus, and N the power-law exponent $(0 \leq N < 1)$. The special case of $N = 0$ corresponds to an elastic-perfect plastic solid.

The true (Cauchy) stresses in a spherical symmetric state can be resolved into a pure hydrostatic stress state and a pure uniaxial one,

$$(\sigma_\mathrm{r}, \sigma_\theta, \sigma_\phi) = (\sigma_\theta, \sigma_\theta, \sigma_\theta) + (\sigma_\mathrm{r} - \sigma_\theta, 0, 0).$$

Since the hydrostatic stress does not produce any strains in an incompressible solid, the uniaxial portion of the stress $(\sigma_\mathrm{r} - \sigma_\theta)$ is directly related to the radial strain ε_r. Therefore Equation A.6 may be rewritten as

$$\frac{\sigma_\mathrm{r} - \sigma_\theta}{\sigma_0} = H(\varepsilon_r). \tag{A.8}$$

In fact, $(\sigma_\mathrm{r} - \sigma_\theta)$ is the Mises stress and ε_r is the effective strain, up to a sign.

With the use of Equation A.1, the radial strain ε_r in (A.3) may be expressed as follows

$$\varepsilon_\mathrm{r} = \frac{2}{3}\ln\frac{r^3 - r_1^3 + R_1^3}{r^3}. \tag{A.9}$$

At the void surface $r = r_1$, the radial strain in Equation A.9 is

$$\varepsilon_\mathrm{r}(r = r_1) = \frac{2}{3}\ln\frac{R_1^3}{r_1^3} = \frac{2}{3}\ln\rho^{-3} = \frac{2}{3}\ln\left(\frac{f_0}{f}\frac{1 - f}{1 - f_0}\right) \equiv \varepsilon_1. \tag{A.10}$$

At the surface $r = r_2$,

$$\varepsilon_r(r = r_2) = \frac{2}{3}\ln\left(\frac{1-f}{1-f_0}\right) \equiv \varepsilon_2. \qquad (A.11)$$

Equations A.10 and A.11 show that the radial strains at the two surfaces of the microvoid cell can be determined from the current and initial void volume fractions.

Using Equation A.9, the governing equation (A.4) may be rewritten as

$$\frac{d\sigma_r}{d\varepsilon_r} = \frac{\sigma_0 H(\varepsilon_r)}{1 - \exp\left(1 - \frac{3}{2}\varepsilon_r\right)}. \qquad (A.12)$$

Integration of Equation A.12 from ε_1 to ε_2 yields

$$\frac{\sigma_r^A + p}{\sigma_0} = \int_{\varepsilon_1}^{\varepsilon_2} \frac{H(\varepsilon)\,d\varepsilon}{1 - \exp\left(-\frac{3}{2}\varepsilon\right)} \stackrel{\text{def}}{=} \mathcal{F}(f; f_0, \varepsilon_0, N) \qquad (A.13)$$

which is a function of the void volume fraction f with f_0, ε_0 and N as parameters. It may be noted that the integral in (A.13) is the same as that given by Huang *et al*. [14]. Also, the use of ε_1 and ε_2 as limits of integration is useful because they are independent of thermal expansions (see, Section 3).

Equation A.13 establishes a relation between the current void volume fraction f and the sum of the internal vapor pressure p and the externally imposed radial stress σ_r^A. Similar to what is shown by Huang *et al*. [14], the integral in (A.13) has its maximum at a critical (current) void volume fraction f_{cr}, which can be computed from the extremum condition $\mathrm{d}(\sigma_r^A + p)/\mathrm{d}f = 0$; i.e.

$$\frac{H(\varepsilon_2)}{1 - \exp\left(-\frac{3}{2}\varepsilon_2\right)}\frac{\mathrm{d}\varepsilon_2}{\mathrm{d}f} - \frac{H(\varepsilon_1)}{1 - \exp\left(-\frac{3}{2}\varepsilon_1\right)}\frac{\mathrm{d}\varepsilon_1}{\mathrm{d}f} = 0.$$

Substitution of Equations A.10 and A.11 yields

$$\frac{1}{f - f_0}\left[H(\varepsilon_2) - \frac{f_0}{f}H(\varepsilon_1)\right] = 0. \qquad (A.14)$$

When $f \neq f_0$, the bracketed term in (A.14) is zero, and the critical fraction f_{cr} is well-defined. For the sum of the applied radial stress and vapor pressure to attain the maximum value, the material in the outer region of the cell must be elastic and the material in the inner region must be plastic [22]. Such a critical behavior is attributed to the synergistic interplay between elasticity and plasticity (see, Faleskog and Shih [12]). Also, void growth ($f \geq f_0$) implies $\varepsilon_1, \varepsilon_2 \leq 0$ as seen from (A.10) and (A.11). Thus, Equation A.14 can be explicitly expressed as

$$\frac{\varepsilon_2}{\varepsilon_0} + \frac{f_0}{f}\left(\frac{-\varepsilon_1}{\varepsilon_0}\right)^N = 0. \qquad (A.15)$$

by using (A.7).

References

1. I. FUKUZAWA, S. ISHIGURO and S. NANBU, in Proc. Int. Reliab. Phys. Symp., 1985, p.192.
2. J. E. GALLOWAY and R. MUNAMARTY, *IEEE Trans. Reliability* **44**(3) (1995) 362.
3. X. J. FAN and T. B. LIM, in ASME 1999 International Mechanical Engineering Congress, 11th Symposium on Mechanics of Surface Mount Assemblies, Nashville, Tennessee, 14–19 November.
4. A. A. O. TAY and T. LIN, *IEEE Transactions on Components, Packaging and Manufacturing Technology—Part A* **19**(2) (1996) 186.
5. J. E. GALLOWAY and B. M. MILES, *ibid.* **20**(3) (1997) 274.
6. S. LIU and Y. MEI, *ibid.* **18**(3) (1995) 634.
7. Y. B. PARK and J. YU, in IEEE/CPMT Int'l Electronics Manufacturing Technology Symposium, 1997, p. 12.
8. K. W. LEE and Y. Y. EARMME, *Finite Elements in Analysis and Design* **30** (1998) 81.
9. J. M. BALL, *Phil. Trans. Roy. Soc. London* **A 306** (1982) 577.
10. Y. HUANG, J. R. HUTCHINSON and V. TVERGAARD, *J. Mech. Phys. Solids* **39** (1991) 223.
11. H.-S. HOU and R. ABEYARATNE, *ibid.* **40** (1992) 571.
12. J. FALESKOG and C. F. SHIH, *ibid.* **45** (1997) 21.
13. P. LIU, L. CHENG and Y. W. ZHANG, *IEEE Transactions on Advanced Packaging*, submitted.
14. Y. HUANG, K. X. HU, C. P. YEH, N.-Y. LI and K. C. HWANG, *J. Electronic Packaging* **118** (1996) 229.
15. A. L. GURSON, *J. Engng. Mater. Tech.* **99** (1977) 2.
16. V. TVERGAARD, *Advances in Applied Mechanics* **27** (1990) 83.
17. X. J. FAN and S. Y. ZHANG, *J. Mater. Sci.* **30** (1995) 3483.
18. V. TVERGAARD and A. NEEDLEMAN, *Acta Metall.* **32** (1984) 157.
19. X. J. FAN, in Proceedings of The Fourth China-Japan-USA-Singapore Conference on Biomechanics, edited by G. T. Yang *et al*. (International Academic Publishers, Beijing, 1995) p. 360.
20. L. XIA and C. F. SHIH, *J. Mech. Phys. Solids* **43** (1995) 233.
21. *Idem., ibid.* **43** (1995) 1953.
22. R. HILL, "The Mathematical Theory of Plasticity" (Clarendo Press, Oxford, 1950).

Received 8 August 2000
and accepted 3 August 2001